Infrared and infrared emission spectroscopic study of selected Chinese palygorskites

Hongfei Cheng [a,b], Jing Yang [b], Ray L. Frost [b•], Zeguang Wu [a]

[a] *School of Geoscience and Surveying Engineering, China University of Mining & Technology, Beijing, 100083 China*

[b] *Chemistry Discipline, Faculty of Science and Technology, Queensland University of Technology, 2 George Street, GPO Box 2434, Brisbane, Queensland 4001, Australia*

Abstract

Infrared and infrared emission spectroscopy were used to analyze the difference in structure and thermal behavior of two Chinese palygorskites. The position of the main bands identified in the infrared spectra of the palygorskites studied is similar for these two Chinese samples, but there are some differences in their intensity, which is significant. This discrepancy is attributed to various geological environments in different regions and the existence of impurities. The infrared emission spectra clearly show the structural changes and dehydroxylation of the palygorskites when the temperature is raised. The dehydration of the palygorskites is followed by the loss of intensity of the OH stretching vibration bands in the region 3600-3200 cm^{-1}. Dehydroxylation is followed by the decrease in intensity in the bands between 3700 and 3550 cm^{-1}. Dehydration of pure palygorskite was completed by 600 °C. Partial loss of coordinated water was observed at 400 °C. Infrared emission spectroscopy is an effective method to determine the stability of the mineral.

Keywords Infrared spectroscopy; Infrared emission spectroscopy; Palygorskite; Sepiolite

• Author to whom correspondence should be addressed (r.frost@qut.edu.au)
T: +61 7 3138 2407; F:+61 7 3138 1804

1. Introduction

Palygorskite is a family of fibrous hydrated magnesium silicate with the structural formula $(OH_2)_4(OH)_2Mg_5Si_8O_{20}\cdot 4H_2O$ [1]. It is known to contain a continuous two dimensional tetrahedral sheet, but differs from other layer silicates in the lack of continuous octahedral sheets [2, 3]. Palygorskite is a hydrous Mg- and Al-rich silicate clay mineral with a fibrous morphology that typically occurs as fine grained, poorly crystalline masses [2, 4, 5]. The structure of palygorskite contains ribbons of 2:1 phyllosilicates linked by periodic inversion of the apical oxygen of the continuous tetrahedral sheet every six atoms of Si (three tetrahedral chains) for sepiolite and every four atoms of Si (two tetrahedral chains) for palygorskite [6, 7]. The discontinuous nature of the octahedral sheet allows for the formation of rectangular channels aligned in the direction of the a-axis, which contain some exchangeable Ca^{2+} and Mg^{2+} cations and "zeolitic water". These nanostructured tunnels account in large part for the high specific surface area and excellent sorption properties of palygorskite. In addition it has good mechanical strength and thermal stability.

Palygorskite is an important clay mineral with a wide variety of industrial applications, due to its unique crystal structure and microfibous nature [6, 8]. These properties make palygorskite ideal for reinforcement of polymer materials, which has been recently used for the reinforcement of elastomers, thermoplastic polymers, and biopolymers [9, 10]. Palygorskite also can be used in oil refining, wastewater treatment, removal of odor, drug, and pesticide carriers, catalysts, paper and detergent industries [11-14]. This mineral has some particularly desirable sorptive, colloidal-rheological and

catalytic properties, in comparison with other clay minerals [8]. Technological applications are based on its physicochemical, principally on structure, composition, thermal behavior, surface area, among others, and especially the structure and thermal stability. In general, lots of the industrial raw palygorskite from China is a mixture of minerals, which contains different nonclay minerals besides major and minor clay minerals. The palygorskites clay in this study from China with the major clay mineral palygorskite includes minor carbonates with dolomite and calcite as nonclay minerals. Therefore, it is highly interest to study the structural analysis and thermal behavior of palygorskites from China.

Although the extensive use of palygorskite in industrial processes and its excellent characteristics for the preparation of organic/inorganic complexes, there is little information about the structural analysis and thermal stability of palygorskite, particularly for the industrial raw palygorskite from China. However, thermal treatment of palygorskite is necessary for its further industrial application, especially in the rubber industry. Infrared emission spectroscopy allows the study of the decomposition, dehydration and dehydroxylation of palygorskite at elevated temperatures. This measurement of discrete vibrational frequencies emitted by thermally excited molecules, known as Fourier transform infrared emission spectroscopy has not been widely used for the study of thermal stability and structure of clay minerals [15-18]. Thermal decomposition analysis using infrared emission spectroscopy technique enables the thermal transformation of minerals, the modification of the structure and the mechanism in response to heat treatment to be determined [17, 19-22]. It has proven extremely useful

for determining the stability of minerals [16, 23]. To the best of the authors knowledge few infrared emission spectroscopic analysis of palygorskite have been undertaken; although differential thermal decomposition analysis and infrared spectroscopic study of palygorskite have been published. This paper reports the structural analysis and thermal decomposition analysis of two palygorskites samples of different origin and with different amount of impurities using infrared (IR) spectroscopy and infrared emission spectroscopy (IES).

2. Experimental methods

2.1 Materials

Two palygorskite samples from Feidong, Anhui province of China and Zhangze, Jiangsu province of China, containing impurities of quartz and dolomite, were selected for this study (Table 1). The samples were used directly, without prior size fraction separation, since one of the objectives was to determine the influence on the thermal behavior of the unmodified mineral samples.

2.2 X-ray diffraction

X-ray diffraction patterns were collected using a PANalytical X'Pert PRO X-ray diffractometer (radius: 240.0 mm). Incident X-ray radiation was produced from a line focused PW3373/10 Cu X-ray tube, operating at 40 kV and 40 mA, with Cu Kα radiation of 1.540596 Å. The incident beam passed through a 0.04 rad soller slit, a 1/2 ° divergence slit, a 15 mm fixed mask, and a 1 ° fixed antiscatter slit.

2.3 Infrared spectroscopy

Infrared spectra were obtained using a Nicolet Nexus 870 FTIR spectrometer with a smart endurance single bounce diamond ATR cell. Spectra over the 4000-650 cm^{-1} range were obtained by the co-addition of 64 scans with a resolution of 4 cm^{-1} and a mirror velocity of 0.6329 cm/s. Spectra were co-added to improve the signal to noise ratio. No sample preparation was involved.

Band component analysis was undertaken using the Jandel'Peakfit'(Erkrath, Germany) software package which enabled the type of fitting function to be selected and allowed specific parameters to be fixed or varied accordingly. Band fitting was done using a Lorentz-Gauss cross-product function with the minimum number of component bands used for the fitting process. The Lorentz-Gauss ratio was maintained at values greater than 0.7 and fitting was undertaken until reproducible results were obtained with squared correlations (r^2) greater than 0.998. Band fitting of the spectra is quite reliable providing there is some band separation or changes in the spectral profile.

2.4 Infrared emission spectroscopy

FTIR emission spectroscopy was carried out on a Nicolet Nexus 870 FTIR spectrometer, which was modified by replacing the IR source with an emission cell. A description of the cell and principles of the emission experiment have been published elsewhere [15-18, 24]. Approximately 0.2mg of palygorskite sample was spread as a thin layer on a 6 mm diameter platinum surface and held in an inert atmosphere within a nitrogen-purged cell during heating. The infrared emission cell consists of a modified atomic absorption graphite rod furnace, which is driven by a thyristor-controlled AC power supply capable of delivering up to 150 A at 12 V. A platinum disk acts as a hot

plate to heat palygorskite sample and is placed on the graphite rod. An insulated 125 -μm type R thermocouple was embedded inside the platinum plate in such a way that the thermocouple junction was less than 0.2mm below the surface of the platinum. Temperature control of ±2 °C at the operating temperature of the sample was achieved by using a Eurotherm Model 808 proportional temperature controller, coupled to the thermocouple.

In the normal course of events, three sets of spectra are obtained over the temperature range selected and at the same temperatures; those of the black body radiation, the platinum plate radiation, and the platinum plate covered with the sample. Normally only one set of black body and platinum radiation is required. The emission spectrum at a particular temperature was calculated by subtraction of the single beam spectrum of the platinum backplate from that of the platinum covered with the sample, and the result ratioed to the single beam spectrum of an approximate black body (graphite). This spectral manipulation is carried out after all the spectral data has been collected.

The emission spectra were collected at intervals of 50 °C over the range 100-1000 °C. The time between scans (while the temperature was raised to the next hold point) was approximately 100s. It was considered that this was sufficient time for the heating block and the powdered sample to reach temperature equilibrium. The spectra were acquired by co-addition of 128 scans for the whole temperature range, with an approximate scanning time of 1 min, and a nominal resolution of 4 cm^{-1}. Good quality spectra can be obtained providing the sample thickness is not too large. If too large a sample is used then the spectra become difficult to interpret due to the presence of

combination and overtone bands. Spectral manipulation such as baseline adjustment, smoothing and normalization was performed using the Spectra calc software package (Galactic Industries Corporation, NH, USA).

3. Results and discussion

3.1 X-ray diffraction (XRD)

The XRD patterns of these two palygorskite samples together with standard XRD patterns are shown in Fig. 1. The XRD pattern of the sample F-1 shows identical pattern to the palygorskite standard, with minor quartz. The sample Z-1 shows impurities of quartz and dolomite. Three sharp strong reflections at 2θ=8.32, 26.62 and 30.86 are due to the palyorskite (P), Quartz (Q) and dolomite (D). It is found that palygorskite sample F-1 is more pure and better crystalline than Z-1. Analysis of the XRD patterns for these two samples reveals that they have palygorskite as the major component. Changes in the relative proportions of the clay minerals can be seen from Fig.1.

3.2 Infrared spectroscopy

The infrared spectra of two Chinese palygorskite samples are shown in Fig. 2 and 3. The two samples exhibit many similarities in the infrared spectra, best observed by comparing these two spectra. Some variations in both the band positions and intensities of the OH, Si–O group vibrational modes and some impurities among these two palygorskites are observed. Moreover, the spectral differences and band component analysis are found to be very useful in order to differentiate these palygorskites. For convenience, the infrared spectra of these two palygorskites are divided into two sections; they are (a) the 3750-2750 cm^{-1} region attributed to OH and Si-OH stretching vibration

142 modes (Fig.2); (b) the 1750-1250 cm^{-1} region due to the impurities and the
143 aluminosilicate framework (Fig.3).
144
145 The infrared spectra of two palygorskites in the 3750-2750 cm^{-1} region are shown in
146 Fig. 2. Eight bands are observed for these two palygorskite samples at 3625, 3612, 3590,
147 3550, 3490, 3380, 3266 and 3203 cm^{-1}. The bands observed at 3625, 3590 and 3550
148 cm^{-1} are in good agreement with the work from Frost [25] and these three bands are
149 assigned to Al_2-OH. This is in agreement with the high amount of Al present in the
150 palyorskite. The band at 3612 cm^{-1} is described in bibliographic references [8, 18, 25, 26]
151 on IR of palyorskite and it seems to be characteristic of this mineral. Furthermore, the
152 band at 3590 cm^{-1} is characteristic of dioctahedral minerals [27]. It is probable that
153 difference in the band position may arise from variations in the mineral composition,
154 sample origin and impurities. According Chahi [26] and Frost [25], the band at 3550
155 cm^{-1}, based on comparison with smectite, is attributed to the stretching vibration of
156 Al-Fe^{3+}-OH or Al-Mg-OH band. As reported by Frost [32] and Suarez [33], in the
157 structure of palygorskite, four water molecules are bonded to Mg^{2+} cations at the both
158 ends of each ribbon and located in the nanopores. These molecules are called
159 coordinated (structural or crystal) water in palygorskite. Furthermore, four water
160 molecules per half-unit cell are located two per two with in the nanocahannels in the
161 both sides of each other ribbon. These water molecules are in hydrogen bonding with
162 coordinated water and each are called zeolitic water. Bands at 3490 and 3203 cm^{-1} are
163 observed. These bands reported by Hayashi [28] are attributed to zeolitic water. With
164 respect to the four bands centered at 3380 and 3266 cm^{-1}, as can be seen in Fig. 2, these

two samples are similar in position but not in intensity. Therefore, the bands observed at 3380 and 3266 cm^{-1} are due to coordinated water in the palygorskite structure. These also are in good agreement with the literature with the assignment of bands to water (coordinated and zeolitic water) [8, 25].

The infrared spectra of two palygorskites in the 1750-750 cm^{-1} region are shown in Fig. 3. The two palygorskite samples exhibit nearly identical bending modes of H_2O triplets at ca.1681, 1660 and 1635 cm^{-1}. These bands studied here are similar in position but not in intensity. This variability may be attributed to differences in origin and with different amount of impurities. It is reported that the presence of two partially resolved bands at 1658 and 1630, which correspond to bending modes of absorbed and zeolitic water. The band observed at 1658 cm^{-1} is attributed to water that is very strongly bound, as would be expected from water coordinated to the magnesium [18]. This result is consistent with the results discussed above. However, significant differences are observed in 1550-1350 cm^{-1} region of the spectrum: the spectrum of sample Z-1 shows a broader band at 1490 cm^{-1} and two weaker bands at 1490 and 1390 cm^{-1}. These three bands are assigned to the $(CO_3)^{2-}$ antisymmetric and symmetric stretching modes [15]. This result is in good agreement with XRD patterns, thus suggesting for successful application of these palygorskites, impurities such as carbonate and sulfate that were not removed during mining must be removed from palygorskite by chemical treatment before it can be further processed.

The spectra in 1350-750 cm^{-1} region for these two palygorskite samples, the most

intense bands cantered at 980 and 1030 $cm^{-1}$are assigned to deformation vibration of OH and stretching of the Si-O units, respectively, which are similar in position and intensity for these two samples. Another band at 1128 cm^{-1} corresponds to the stretching of the Si-O units. The characteristic band of palygorskite is observed at 1195 cm^{-1}, which is in good agreement with the research by Suarez [8]. The band centered at 912 cm^{-1} in these two palygorskite samples is assigned to the Al-OH-Al deformation, and it is a consequence of the dioctahedral character of palygorskite [26, 29]. This result is in a good agreement with the discussion above. The band centered at 894 cm^{-1} is attributed to vibrational modes of band Al-Fe-OH [26]. Another band at 1097 cm^{-1} is observed in these two palygorskite samples. One possible assignment of this band is to the stretching vibration of M-O.

The infrared spectra showed hydroxyl stretching at 3620, 3590 and 3550 cm^{-1} for the palygorskite and at 3480, 3380, 3266 and 3190 cm^{-1} for the two kinds of water in the structure of palygorskite. Several bands are observed between 1350 and 750 cm^{-1} region. These bands are the basic structure of palygorskite. In general, the bands discussed above for palygorskite seem to be characteristic of this mineral. The differences are found between almost pure palygorskite sample F-1 and the palygorskite with some impurities sample Z-1.This discrepancy is attributed to the existence of impurity.

3.3 Infrared emission spectroscopy

Infrared emission spectroscopy allows the possibility of confirmation of those bands observed in the infrared spectra. Further, the use infrared emission spectroscopy may allow the determination of the bands which are due to contaminants in the palygorskite.

212 The infrared emission spectra of two Chinese palygorskite samples are shown in Fig. 4a
213 and b. The spectra clearly show the changes of structure that occur upon heating. Thus
214 OH stretching vibrations are observed in the 3750-3150 cm^{-1} region, and bending modes
215 of H_2O and the vibrations of the aluminosilicate framework in 1750-650 cm^{-1} region.
216 Since these changes can be most clearly seen for the changes on the basic structure,
217 especially the effect on vibrations of OH coordinated to the octahedral ion pair Al,Al at ca.
218 3627 cm^{-1}, the discussion will be centered around these emission bands. For convenience,
219 the infrared spectra of these two palygorskites also are divided into two sections; they are
220 (a) the 3750-2750 cm^{-1} region attributed to OH and Si-OH stretching vibration modes
221 (Fig. 5 a and b); (b) the 1750-1250 cm^{-1} region due to the impurities and the
222 aluminosilicate framework (Fig. 6 a and b).
223
224 In order to follow these thermal decomposition three spectra at 200, 400 and 600 °C
225 were selected for further analysis. The infrared emission spectra of two Chinese
226 palygorskite samples at 200, 400 and 600 °C in the 3750-2750 cm^{-1} range are shown in
227 Fig. 5 a and b. Interpretation of structural changes in palygorskite by infrared emission
228 spectroscopy during folding is greatly facilitated by decrease of intensities of these bands.
229 At 200 °C, when the zeolitic water has been lost, the absorption band at 3625 cm^{-1}
230 decrease in intensity and two new bands 3643 and 3660 cm^{-1} appear, due to the new
231 environment created for the Al-Al-OH during folding. Two bands at 3490 and 3203 cm^{-1}
232 disappeared, this result proves they are attributed to zeolitic water again and is in good
233 agreement with the other reports about the zeolitic water lost below 200 °C [30-32]. The
234 other bands also are observed at 3533, 3475, 3388, 3293 and 3239 cm^{-1} for sample F-1

and at 3534, 3467 and 3376 cm^{-1} for samples Z-1, due to the coordinated water. In the sample Z-1, another band observed at 3617 cm^{-1}, which is due to the impurity influencing on structural hydroxyl stretching of palygorskite. Two bands disappeared for sample Z-1 below 200 °C. This probably is because the sample Z-1 with some impurity is less crystalline and would have more exterior edges. Therefore, it is easy to lose water in the structure of palygorskite with some impurities. This result is in good agreement with VanScoyoc' report [7]. After heating the samples to 400 °C, thus removing partially coordinated water, two bands are observed at 3533 and 3385 cm^{-1} for sample F-1, at 3534 and 3446 cm^{-1} for sample Z-1. The infrared emission spectra of palygorskite samples illustrate that continued heating of F-1 almost pure palygorskite sample to 600 °C results in loss of the remaining coordinated water and the structural hydroxyls, but for the sample Z-1 results in loss of two kinds of water and only partial of structural hydroxyl. As the sample Z-1 is dehydroxylated at 600 °C, the stretching vibrational bands decrease intensity, but not completely disappear, indicating that the thermal dehydration of palygorskite minerals, especially the coordinated water and structural hydroxyl, is decided not only by the main physicochemical properties of palygorskite, but also by the mount and kind of impurities.

The infrared emission spectra at 200, 400 and 600 °C for these two palygorskite samples in the 1750-650 cm^{-1} range are shown in Fig. 6 a and b. The band intensities from infrared absorption spectroscopy differ from the infrared emission spectroscopy values reported here. This is not unexpected, as infrared emission intensities are not necessarily the same as infrared absorption intensities even though the band centers occur

in similar positions. In the 200 °C spectra for these two samples, the bands observed at 1671, 1635 and 1614 cm^{-1} for F-1 and only 1635 cm^{-1} for Z-1, which are assigned to the bending modes of coordinated water in the structure of palygorskite. After heating the samples to 400 °C, the decrease of intensities of these bands gives rise to the loss of partial coordinated water. This result corresponds to that discuss above. Three bands corresponded to the $(CO_3)^{2-}$ antisymmetric and symmetric stretching modes are also observed in the infrared emission spectroscopy. It is shown that these bands disappear below 600 °C. The other bands in the 1250-650 cm^{-1} range are observed. However, the low wavenumber bands, which are not observed in infrared spectra for these two samples, are observed in infrared emission spectra at 200 and 400 °C. According to the research by VanScoyoc [7], when the samples are heated, partial coordinated water molecules is removed from the octahedral magnesium, the structure folds. The remaining coordinated water is then forced closer to the hexagonal hole of the amphibole chain. Thus, the palygorskites are in a disordered state at this temperature range. Therefore, the low wavenumber bands of these two palygorskites are due to the structural changes of aluminosilicate framework and magnesium on heating. It also has been proposed that the loss of the partial structural water is accompanied by a partial collapse of the structure [33]. Considerable differences are found between the values of bands at room temperature and those at 600 °C. This is because when the anhydride is formed, however, the edge magnesium completes its coordination with the two nearest oxygens of the neighboring silica surface which has been brought into close proximity by the folding [34].

Comparing these two palygorskite minerals, F-1 sample shows the typical infrared emission bands and thermal decomposition process as above. However, palygorskite sample Z-1, regardless of the content of mainly composition, exhibited several additional bands of the spectrum and different thermal behavior. These results suggest that the infrared emission spectrum of palygorskite mineral from different region is decided not only by the main physicochemical composition of palygorskite, but also by the mount and kind of impurities.

4. Conclusions

Infrared spectroscopy and infrared emission spectroscopy are used to study the difference in the structure and thermal behavior between the almost pure palygorskite sample F-1 and the palygorskite sample Z-1 with some impurities. Several types of water molecules were observed in this mineral. The infrared spectra showed hydroxyl stretching at 3620, 3580 and 3550 cm^{-1} for the palygorskite and at 3480, 3380, 3266 and 3190 cm^{-1} for the water in the structure of palygorskite. The bands are observed between 1250 and 750 cm^{-1} region. These bands are the basic structure of palygorskite. There are some differences in these two Chinese palygorskites.

Infrared and Infrared emission spectra have shown that drastic structural changes occur in two Chinese palygorskites during dehydration. However, most of these changes occur prior to complete dehydration. Infrared emission spectroscopy shows that during dehydration all the structural hydroxyl and coordinated water have shift to a new environment. The temperature of dehydration and dehydroxylation of palygorskite is influenced by the geological environment and the amount and kind of impurities. Therefore, impurities such as carbonate and sulfate that were not removed during mining

must be removed from palygorskite by chemical treatment before it can be further processed.

Acknowledgment

The authors gratefully acknowledge the financial support provided by the National Natural Science Foundation of China (51034006) and infra-structure support of the Queensland University of Technology, Chemistry Discipline, Faculty of Science and Technology.

References

[1] W.F. Bradley, Am Mineral 25 (1940) 405.
[2] C.L. Christ, J.C. Hathaway, P.B. Hostetler, A.O. Shepard, Am Mineral 54 (1969) 198.
[3] N. Güven, J.-B.d.E.d.l. Caillerie, J.J. Fripiat, Clay Clay Miner 40 (1992) 457.
[4] J.J. Beaudoin, P.E. Grattan-Bellew, Cement Concrete Res 10 (1980) 347.
[5] C. Blanco, F. González, C. Pesquera, I. Benito, S. Mendioroz, J.A. Pajares, Spectrosc Lett 22 (1989) 659
[6] W. Kuang, G.A. Facey, C. Detellier, Clay Clay Miner 52 (2004) 635.
[7] G.E. VanScoyoc, C.J. Serna, J.L. Ahlrichs, Am Mineral 64 (1979) 215.
[8] M. Suarez, E. Garcia-Romero, Appl Clay Sci 31 (2006) 154.
[9] L. Bokobza, J.-P. Chauvin, Polymer 46 (2005) 4144.
[10] A. Arques, A.M. Amat, L. Santos-Juanes, R.F. Vercher, M.L. Marín, M.A. Miranda, J Mol Catal A:Chem 271 (2007) 221.
[11] M.E. Sedaghat, M. Ghiaci, H. Aghaei, S. Soleimanian-Zad, Appl Clay Sci 46 (2009) 131.
[12] M. Onal, Y. Sarikaya, Appl Clay Sci 44 (2009) 161.
[13] S. Kocaoba, Desalination 244 (2009) 24.
[14] Z.-Q. Lei, S.-X. Wen, Eur Polym J 44 (2008) 2845.
[15] R.L. Frost, S. Bahfenne, J. Graham, Spectrochim Acta A: Mol Biomol Spectrosc 71 (2008) 1610.
[16] R.L. Frost, J.T. Kloprogge, Spectrochim Acta A: Mol Biomol Spectrosc 55 (1999) 2195.
[17] R.L. Frost, M.L. Weier, Thermochim Acta 406 (2003) 221.
[18] R.L. Frost, G.A. Cash, J.T. Kloprogge, Vib Spectrosc 16 (1998) 173.
[19] R.L. Frost, M.L. Weier, J Raman Spectrosc 35 (2004) 299.
[20] R.L. Frost, S.J. Mills, K.L. Erickson, Thermochim Acta 419 (2004) 109.
[21] J.T. Kloprogge, L. Hickey, R.L. Frost, Appl Clay Sci 18 (2001) 37.
[22] R.L. Frost, S.M. Dutt, J Colloid Interface Sci 198 (1998) 330.
[23] R.L. Frost, M.L. Weier, W. Martens, J Therm Anal Calorim 82 (2005) 373.
[24] R.L. Frost, D. Wain, J Therm Anal Calorim 91 (2008) 267.
[25] R.L. Frost, O.B. Locos, H. Ruan, J.T. Kloprogge, Vib Spectrosc 27 (2001) 1.
[26] A. Chahi, S. Petit, A. Decarreau, Clay Clay Miner 50 (2002) 306.
[27] C. Serna, G.E. VanScoyoc, J.L. Ahlrichs, Am Mineral 62 (1977) 784.
[28] H. Hayashi, R. Otsuka, N. Imai, Am Mineral 54 (1969) 1613.
[29] J. Madejová, P. Komadel, Clay Clay Miner 49 (2001) 410.
[30] R. Nagata, S. Shimoda, T. Sudo, Clay Clay Miner 22 (1974) 285.
[31] V. Gionis, G.H. Kacandes, I.D. Kastritis, G.D. Chryssikos, Am Mineral 91 (2006) 1125.
[32] J.E. Post, P.J. Heaney, Am Mineral 93 (2008) 667.
[33] A. Preisinger, Clay Clay Miner 10 (1963) 365.
[34] C. Serna, J.L. Ahlrichs, J.M. Serratosa, Clay Clay Miner 23 (1975) 452.

LIST OF TABLES

Table 1

Palygorskite Samples	Location	Content of clay mineral	Impurities
Palygorskite(F-1)	Feidong, Anhui province of China	Palygorskite	Quartz
Palygorskite(Z-1)	Zhangze, Jiangsu province of China	Palygorskite	Quartz, Dolomite

LIST OF FIGURES

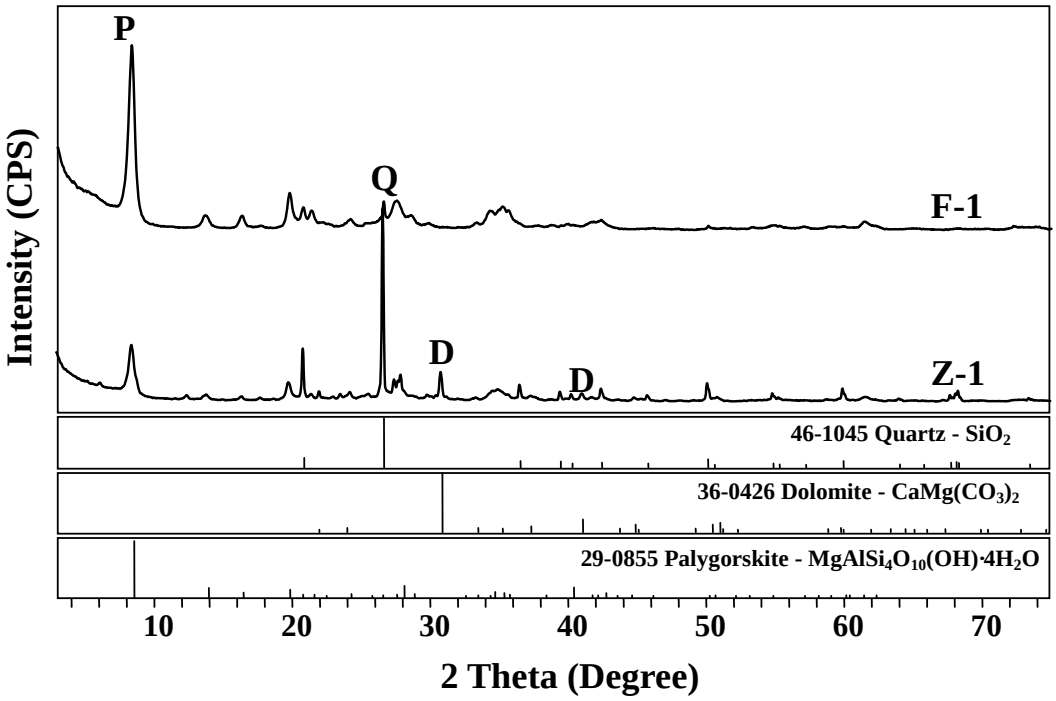
P
Q
D
D
F-1
Z-1
Intensity (CPS)
46-1045 Quartz - SiO2
36-0426 Dolomite - CaMg(CO3)2
29-0855 Palygorskite - MgAlSi4O10(OH)·4H2O
10
20
30
40
50
60
70
2 Theta (Degree)

Fig.1

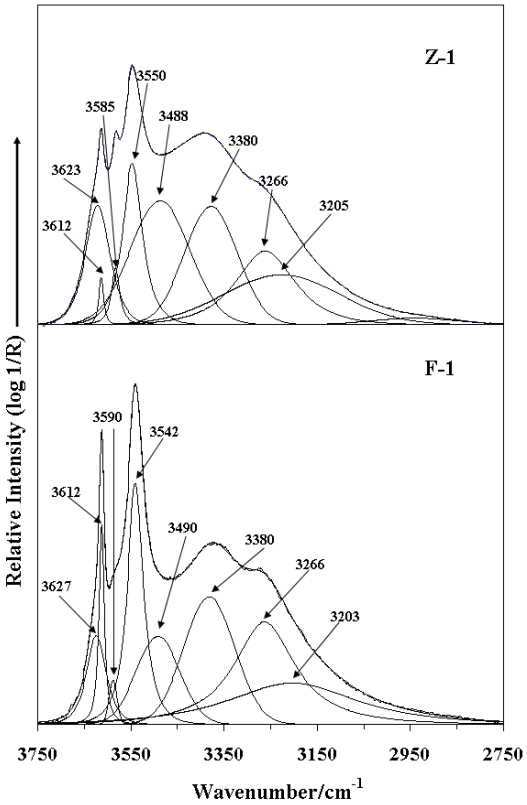
Z-1
3550
3585
3488
3380
3623
3266
3205
3612
F-1
3590
3542
3612
3490
3380
3266
3627
3203
Relative Intensity (log 1/R)
3750
3550
3350
3150
2950
2750
Wavenumber/cm-1

Fig.2

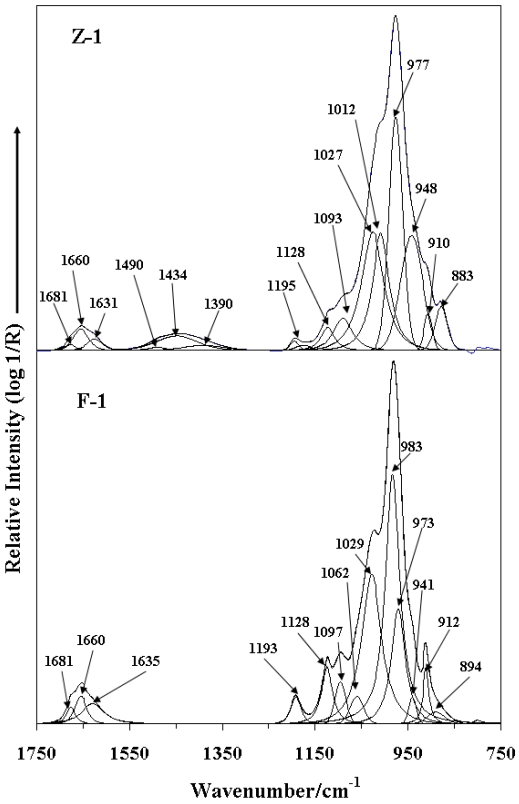
Z-1
977
1012
1027
948
1093
910
1128
883
1660
1490
1434
1195
1681
1631
1390
F-1
983
973
1029
1062
941
1128
912
1097
1660
1193
1681
1635
894
Relative Intensity (log 1/R)
1750
1550
1350
1150
950
750
Wavenumber/cm-1

Fig.3

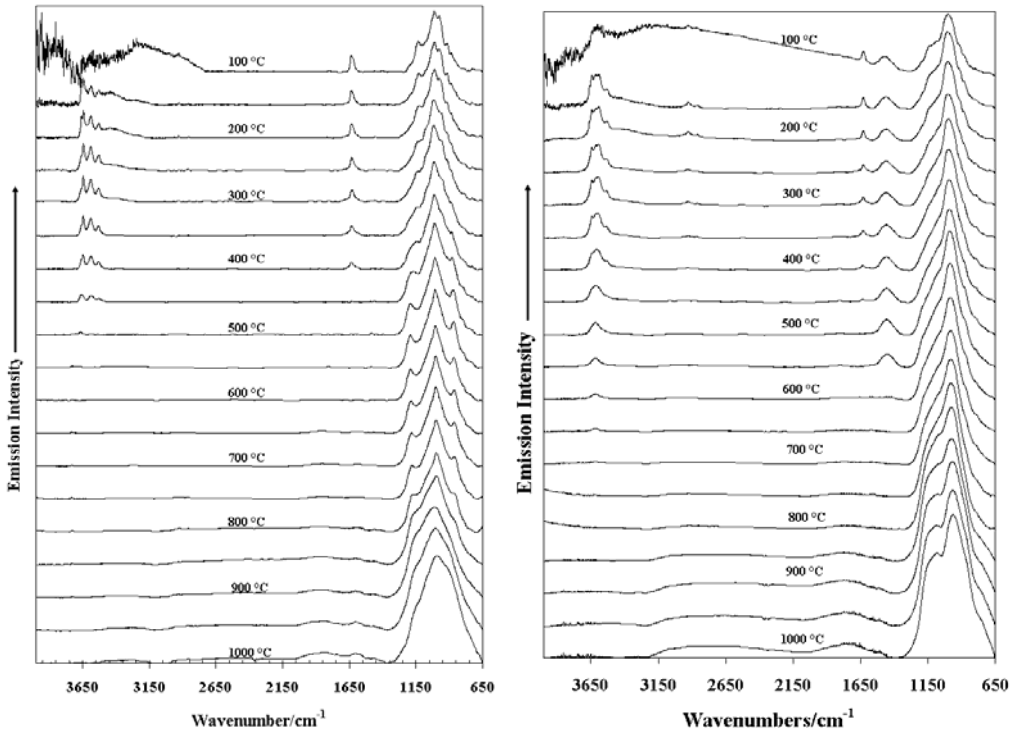
100 °C
200 °C
300 °C
400 °C
500 °C
600 °C
700 °C
800 °C
900 °C
1000 °C
Emission Intensity
3650
3150
2650
2150
1650
1150
650
Wavenumber/cm-1
Wavenumbers/cm-1

a b

Fig. 4

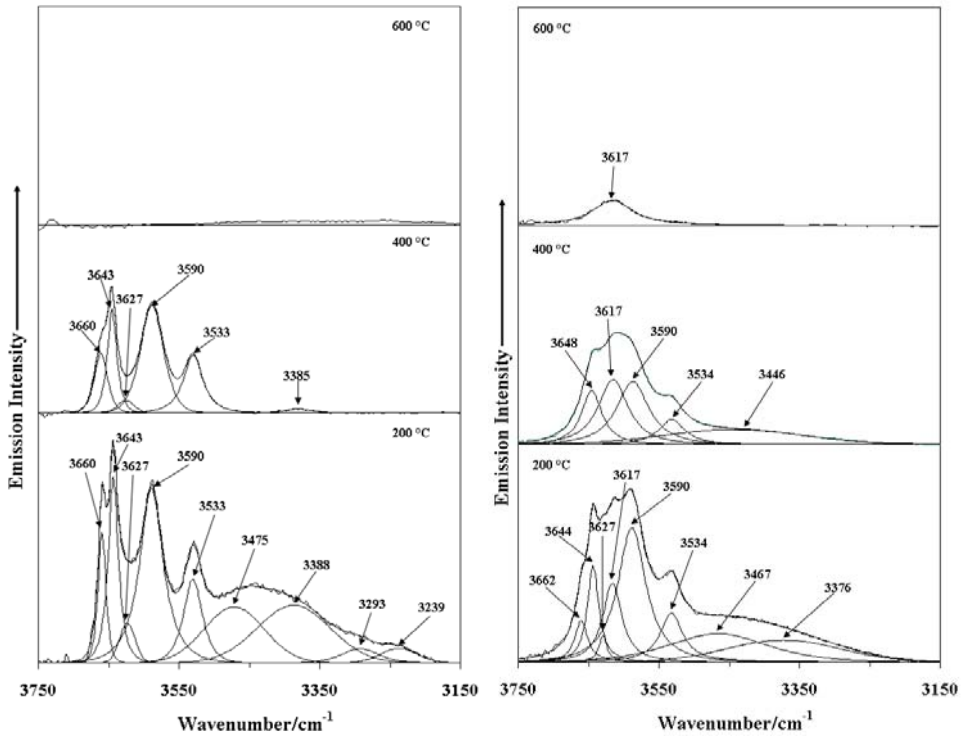
600 °C
400 °C
200 °C
3643
3627
3660
3590
3533
3385
3475
3388
3293
3239
Emission Intensity
3750
3550
3350
3150
Wavenumber/cm-1
600 °C
3617
400 °C
3617
3590
3648
3534
3446
200 °C
3617
3590
3644
3627
3534
3662
3467
3376
Emission Intensity
3750
3550
3350
3150
Wavenumber/cm-1

a b

Fig. 5

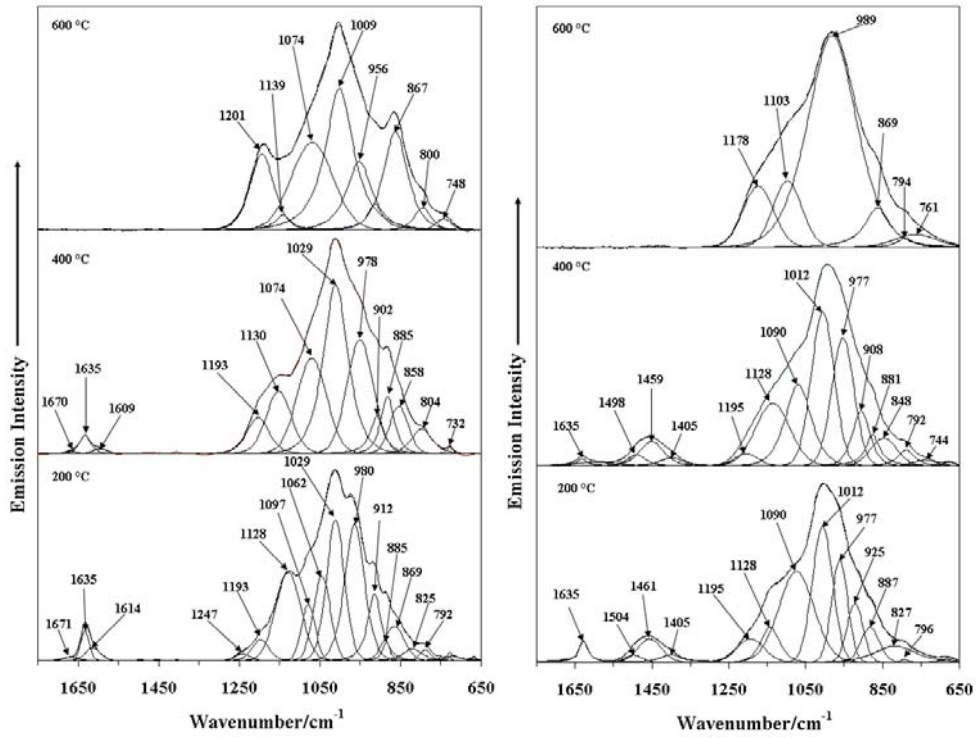
600 °C
1009
1074
1139
956
867
1201
800
748
400 °C
1029
978
1074
902
1130
885
1193
1635
858
1670
1609
804
732
200 °C
1029
980
1062
1097
912
1128
885
1635
869
1193
825
1614
1671
1247
792
1650
1450
1250
1050
850
650
Wavenumber/cm-1
Emission Intensity
600 °C
989
1103
869
1178
794
761
400 °C
1012
977
1090
908
1459
1128
881
1498
1195
848
1635
1405
792
744
200 °C
1012
1090
977
925
1128
1461
1195
887
1635
1504
827
1405
796
1650
1450
1250
1050
850
650
Wavenumber/cm-1
Emission Intensity

a b

Fig. 6